Chinese Chemical Letters
journal homepage: www.elsevier.com

Communication

Oxide-supported Metal Catalysts for Anaerobic NAD^+ Regeneration with Concurrent Hydrogen Production

Jianwei Li,[a] Joseph W.H. Burnett,[a] Claudia Martinez Macias,[a] Russell F. Howe,[b] and Xiaodong Wang[a,*]

[a]*Chemical Engineering, School of Engineering, Lancaster University, Lancaster LA1 4YW, United Kingdom*
[b]*Chemistry Department, University of Aberdeen, Aberdeen AB24 3UE, United Kingdom*

ARTICLE INFO

Article history:
Received
Received in revised form
Accepted
Available online

Keywords:
NAD^+ regeneration
Heterogeneous catalyst
Hydrogenase mimic
Hydrogen binding energy
Hydrogen production

ABSTRACT

We report SiO_2-supported monometallic Pt, Pd, Au, Ni, Cu and Co catalysts for proton-driven NAD^+ regeneration, co-producing H_2. All metals are fully selective to NAD^+ where the order of turnover frequencies (Pt > Pd > Cu > Au, Ni and Co) coincides with those otherwise observed in electrochemical hydrogen evolution reactions. This has revealed that NADH is capable of converting the metal sites into a "cathode" without an external potential and the NADH to NAD^+ reaction involves transferring electron and hydrogen atom separately. Electron-deficient $Pt^{\delta+}$ (on CeO_2) enhances TOF and the heterogeneous Pt/CeO_2 catalyst is recyclable without losing any activity/selectivity.

Biocatalysis using enzymes has attracted increasing interest in recent decades due to its outstanding activity and chemo-, regio- and stereo-selectivity in biosensor, pharmaceutical and organic synthesis [1-2]. As most enzymes intrinsically work under benign conditions, they are also able to lower energy costs, avoid extreme pH requirements as well as reduce environmental hazards [3-8]. Dehydrogenases (DHs) are a group of important enzymes that catalyze reversible oxidative transformations of hydroxyls and amines (Fig. 1a), some of which are novel reaction routes over conventional organic synthesis. The usage of DHs is limited by their dependence on the NAD(P)H/$NAD(P)^+$ cofactor pair (Fig. 1b), which act as an electron carrier and is consumed stoichiometrically in enzymatic redox reactions. Due to the high cost of these cofactors (e.g., \$1400 and \$2600 per mol of NAD^+ and NADH, respectively) [9], a regeneration system is essential to make these biosynthetic processes viable (Fig. 1c) [10,11]. Compared to the commercial uses of NAD(P)H and its regeneration, less attention has been paid to the regeneration of $NAD(P)^+$, hampering the application of DH-catalyzed oxidative transformations [12].

To date, enzymatic NAD^+ regeneration using a second enzyme as the regeneration catalyst (e.g. lactate dehydrogenases, glutamate dehydrogenases, NADH oxidases and, particularly, NADH oxidases (NOXs) has been mostly studied [13-16]. Although NOXs can generate H_2O (from O_2) as a clean product [15], the costliness, instability, and difficulty in downstream separation of enzymes remain challenging. New catalytic regeneration approaches based on homogeneous [17,18], electro- [19-21], and photo-catalysis [22-25] have been reported but are still at developmental stages. Improvements are required in regeneration efficiency (selectivity and activity), ease of preparation/separation, and system compatibility [21,26-28].

$$NADH + H^+ \rightarrow NAD^+ + H_2 \quad \text{(Eq. 1)}$$

The use of solid catalysts for NAD^+ regeneration is a newly developed method where only supported Au, Pt and graphene oxide (Cu^{2+} ion-doped) have so far been studied [29-31]. The advantages of using supported metal catalysts lie in their low-cost preparation/setup, ease of separation, recyclability and scaling-up, and stable physicochemical properties. The previously reported catalytic systems were only active when using strong oxidant, molecular O_2. We have recently established a new regeneration pathway employing activated carbon supported Pt that promoted NAD^+ regeneration using the readily available solution protons and concurrently produce H_2 (Eq. 1) [32]. Oxidizing NADH with a proton is more challenging as the latter is a significantly weaker oxidant than O_2 but it offers the possibility of avoiding the O_2-liquid interfacial issues of deactivation [33-38] and has better potential for large scale applications with the further benefit of producing H_2.

* Corresponding author.
E-mail address: xiaodong.wang@lancaster.ac.uk

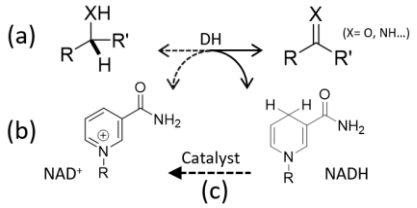

Fig. 1. Schematic of dehydrogenases (DHs)-catalyzed oxidative biotransformations (a), molecular structure of cofactors (b) and catalytic NAD^+ regeneration (c). Solid and dash arrows in (a) represent reversible oxidative and reductive transformations catalyzed by DHs, respectively. R: adenine dinucleotide.

Carbon has been an excellent carrier for cofactor regeneration due to its own capability in electron transfer [39,40]. However, this makes it difficult to decouple the effects of the support and the metal (i.e., Pt, Pd, etc.) which hinders understanding of the role of the metal sites. In this work, we aim to address this gap of knowledge in proton-driven $NAD(P)^+$ regeneration. For the first time, a group of monometallic catalysts comprising Pt, Pd, Au, Ni, Cu and Co supported on non-conductive metal oxides (SiO_2, MgO and CeO_2) have been examined, with the role of metal revealed. Very surprisingly, with its capacity of donating electrons, NADH has effectively made a thermal/heterogeneous catalytic process "electrocatalytic", governed by the hydrogen evolution reactions.

Full details of the materials used, catalyst preparation and characterization procedures are given in the Supporting Information. Catalysts were characterized by chemical analysis, X-ray powder diffraction, transmission electron microscopy, surface area and pore size analysis, and hydrogen temperature-programmed reduction. NAD^+ regeneration reactions were performed as described in the SI. The NADH concentration and conversion were determined by tracing the UV absorbance at 340 nm while the NAD^+ concentration and selectivity were monitored using enzymatic assays described in the SI and in our previous work [41]. The reaction rate constants (k) were determined following first order kinetics. Turnover frequencies (TOF: NADH reacted per surface metal atom per hour) were estimated from the rate constants and the mean particle sizes obtained from TEM analysis, assuming spherical particles. The amount of hydrogen produced was measured volumetrically as described in the SI, and the gas composition confirmed by gas chromatography.

Table 1 summarizes the characterization data for the SBA-15 supported Pt, Pd, Au, Ni, Co and Cu catalysts tested for NAD^+ regeneration in this work. All catalysts showed similar distributions of metal particle sizes (TEM images in Fig. 2) and mean particle diameters of around 4 nm, and nitrogen adsorption/desorption showed negligible pore blockage of the SBA-15 following addition of metal.

The data shown in Fig. 3a are NADH conversions after 1 hour of reaction at pH 7. As illustrated in Fig. 3a, only SBA-15 supported Pt, Pd and Cu give NADH conversions significantly higher than that seen in the absence of catalyst. The uncatalyzed decay of NADH is due to hydration of C=C bonds in the nicotinamide ring, which causes an increase in absorbance at around 290 nm and does not form NAD^+ [42,43]. Fig. S4 illustrates this (homogeneously) acid catalyzed undesirable reaction.

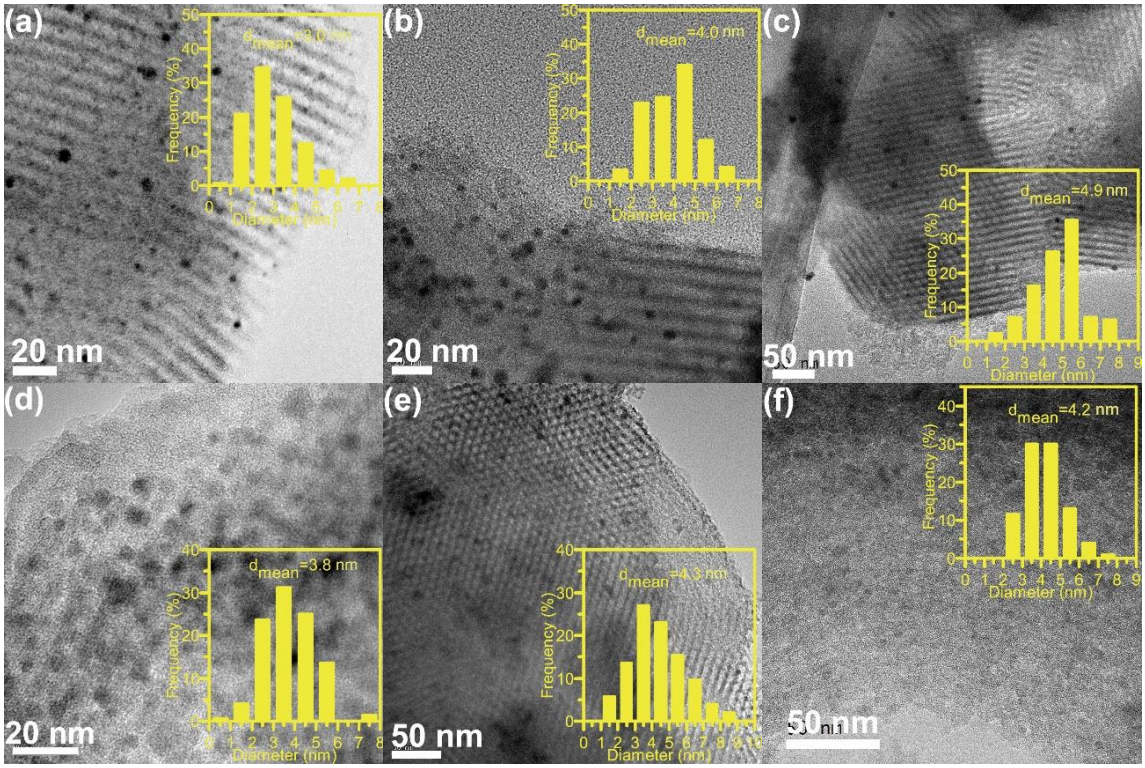

Fig. 2. Representative TEM images and size distribution histograms of the reduced catalysts: Pt (a), Pd (b), Au (c), Ni (d), Co (e) and Cu (f) on SBA-15.

Table 1
Catalyst characterization of all supported metal catalysts used.

	BET surface area ($m^2\ g^{-1}$)	Pore volume ($cm^3\ g^{-1}$)	Metal loading (wt. %)	Particle size range (nm)	Mean diameter (nm)
SBA-15	626.2	0.75	-	-	-
Pt/SBA-15	602.4	0.73	0.99	0.9-6.9	3.0
Pd/SBA-15	614.6	0.70	1.30	1.3-6.9	4.0
Au/SBA-15	607.5	0.60	1.11	1.2-7.8	4.9
Ni/SBA-15	623.4	0.71	0.69	0.9-7.6	3.8
Co/SBA-15	631.5	0.56	0.85	1.1-8.2	4.3
Cu/SBA-15	612.6	0.72	0.94	2.1-7.7	4.2
MgO	68.8	0.52	-	-	-
CeO_2	367.2	0.61	-	-	-
Pt/MgO	46.5	0.47	1.04	1.5-8.2	3.1
Pt/CeO_2	353.6	0.59	1.10 (1.08a)	1.1-7.1	2.9

[a] After recycle test.

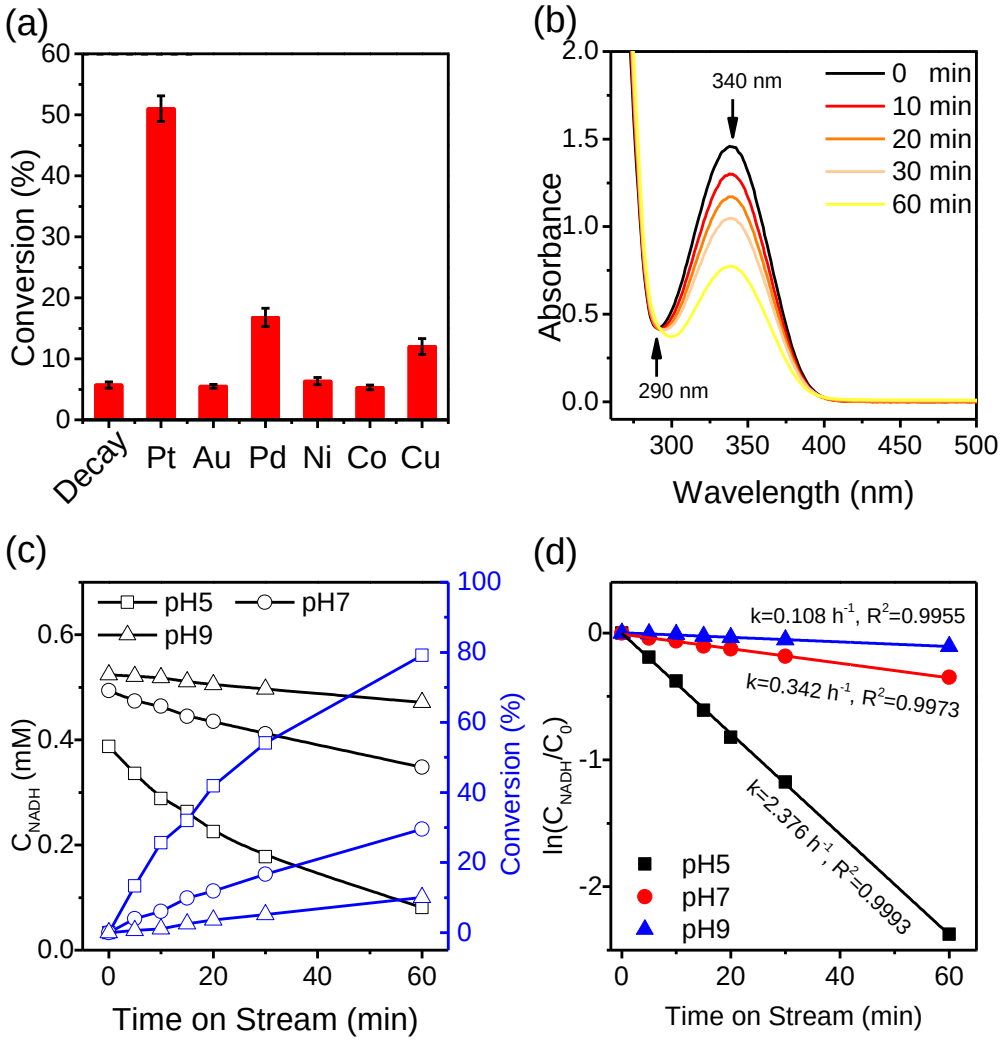

Fig. 3. NAD^+ regeneration promoted by the SBA-15 supported metal catalysts: NADH conversions over different metals (a), UV-VIS spectrum scans of NAD^+ regeneration over Pt/SBA-15 (b), temporal NADH concentration and conversion at different pH over Pt/SBA-15 (c) and first order kinetic plots (d). Reaction conditions: 37 °C, 0.5 mM NADH, pH 7 (for a and b), 100 ml min^{-1} N_2 flow, 1 h, 60mg (a and b) or 30 mg (c and d) of catalyst.

Fig. 3b shows time dependence of the UV-VIS spectrum during NADH conversion over Pt/SBA-15 at pH 7. The decreasing absorbance at 340 nm due to the nicotinamide ring is not accompanied by any change at 290 nm, indicating that the undesired hydration reaction does not occur in the presence of the heterogeneous catalyst. Fig. 3c plots NADH concentration versus time at three different pHs and the corresponding first order plots are given in Fig. 3d. Clearly, an acidic environment gave the highest conversion (i.e., 80% at pH 5, 30% at pH7 and 15% at pH 9). The obvious promoting effect of acidic conditions indicates the participation of H^+ in the regeneration reaction. A further regeneration test in DMSO, a non-proton polar solvent, was carried out in lieu of buffer solution. Since DMSO is incapable of providing H^+, the NADH concentration remained unchanged after 1 h reaction showing the need of a proton for the reaction to occur in contrast to the results obtained for the reaction in a phosphate buffer (Fig. S5). Interestingly, a significant consumption (seen from 340 nm) was observed after an addition (1 ml) of concentrated phosphoric acid. These results further confirm the essential role of protons in the NADH conversion, rather than a sequential step. Nevertheless, the peak rise at 290 nm was also observed which is an indicator of NADH

decay product. This process was inevitable as the concentrated acid also contained water resulting in the hydration of NADH. However, this effect was inconsequential as it happens at a lower rate than that of the catalytic NAD^+ regeneration (as shown by Fig. 3d and S4c). The first order kinetics demonstrated here is contrast with the second order kinetics reported for the oxygen-assisted NADH oxidation over platinum nanoparticles [31], suggesting a different reaction mechanism is operating. The selectivity of the NADH conversion to NAD^+ was determined by enzymatic assay of the NAD^+ concentration. For example, converting 0.255 mM of NADH over Pt/SBA-15 at pH 7 for 1 hour (Fig. 3a) produced 0.25 mM of NAD^+, indicating close to 100% selectivity.

In a separate (scaled up) experiment, the production of hydrogen during the reaction was measured. After 12 hours of reaction at pH 7 with 120 mg of catalyst and an initial NADH concentration of 2 mM, the amount of hydrogen produced (4.2 ml) was close to that expected (4.8 ml) for the observed NADH conversion of 2 mM and the reaction stoichiometry in Eq. 1. Thus, despite the weaker oxidation potential than O_2 (0.82 V for $E^0(O_2/H_2O)$ vs. -0.41 V for $E^0(H^+/H_2)$, at pH7) [44], H^+ was able to drive the regeneration in the presence of Pt. Opposed to the existing O_2-assisted attempts on supported Au and Pt, the catalyst in this work functionally mimicked (NAD(H)-linked) hydrogenases which catalyze the conversion of NADH to NAD^+ and H_2 (Eq. 1).

Two possible scenarios for the mechanism of the reaction in Eq. 1 are illustrated in Fig. 4. The first (Fig. 4a) involves a direct hydride transfer to a proton to form H_2 at the platinum, while the second (Fig. 4b) is an indirect hydride transfer and involves the electron and the extracted/adsorbed hydrogen atom being transferred separately to a proton to form hydrogen. The observed sequence of activities of the different metals supported on SBA-15 (Pt >> Pd > Cu > Ni, Co, Au) is in excellent agreement with that of the electrochemical hydrogen evolution reaction (HER) in which electrons are combined with protons at a cathode to form hydrogen, *via* either the Volmer-Heyrovsky (Eq. 2, 3) or the Volmer-Tafel (Eq. 2, 4) sequences [45-48].

$$\text{Volmer: } H^+ + e^- + * \leftrightarrow H_{ad} \qquad \text{(Eq. 2)}$$

$$\text{Heyrovsky: } H_{ad} + H^+ + e^- \leftrightarrow H_2 + * \qquad \text{(Eq. 3)}$$

$$\text{Tafel: } 2H_{ad} \leftrightarrow H_2 + 2* \qquad \text{(Eq. 4)}$$

The hydrogen binding energy (HBE) has been well established for correlating with the HER activity of metals [45-48]. The high HER activity of platinum is attributed to the optimum hydrogen binding affinity as revealed in the volcano plots (Fig. S6). NADH is a well-known electron donor in nature. When it is continuously supplied/activated on a metal site such as platinum, the surface environment may be considered as mimicking an electrochemical HER at a cathode. Given the excellent agreement in the trends of metal activity between the two types of reaction, it may be argued that a mechanism for NAD^+ regeneration involving steps equivalent to the HER (Fig. 4b) is plausible. The metal acts as a reservoir to accommodate hydrogen atoms (H_{ad}) and transfer electrons. Concertedly, an electron from NADH combines with a proton from the solution which then reacts with H_{ad} to release H_2 (i.e., the Volmer-Heyrovsky process (Eq. 2, 3). Alternatively, two H_{ad} can also react to form H_2 (i.e., the Volmer-Tafel process (Eq. 2, 4). The key is that both processes rely on H_{ad} instead of hydride as an intermediate. Indeed, Attard *et al.* claimed that the formation of hydride on Pt (i.e., Fig. 4a) is thermodynamically unfavorable in aqueous solutions, further supporting the above analysis [49]. The rate determining step of this NADH to NAD^+ conversion is therefore the HER, as opposed to NADH adsorption/activated or NAD^+ desorption.

The electronic properties of oxide supported platinum catalysts are known to be influenced by the nature of the support [50,51]. In Fig. 5a, we have compared the conversion of NADH under the same reaction conditions over SBA-15, CeO_2 and MgO supported platinum. All three catalysts contain similar platinum loadings and the mean particle sizes, and particle size distributions are closely similar (see TEM analyses in Fig. S7c, d), ruling out any effect of particle size on the activity. Additionally, the effect of the oxide supports (coming from different porous structure) was also discarded by examining NADH conversion over bare supports, as shown in Fig. S8. The TOFs estimated from first order plots are respectively 39, 30 and 9 h^{-1} for Pt supported on CeO_2, SBA-15 and MgO. All three catalysts were completely selective to NAD^+ as determined by enzymatic assays. XPS spectra in the 4f region (Fig. 5b) show that platinum on CeO_2 was electron deficient relative to metallic platinum black (Pt $4f_{7/2}$ binding energy of 72.5 eV compared with 71.6 eV for platinum (0), Fig. S9), whereas platinum on SBA-15 has a $4f_{7/2}$ binding energy of 71.6 eV and platinum on MgO 71.4 eV. We suggested that the electron deficient nature of the platinum on CeO_2 led to a reduced hydrogen binding strength, favoring the desorption of hydrogen. Fig. 5c shows the correlation between TOF and Pt $4f_{7/2}$ binding energy. A similar conclusion has been reported concerning the advantage of electron deficient platinum for HER kinetics [52-54].

Finally, we tested the recyclability of the heterogeneous supported Pt catalyst using the most active Pt/CeO_2 as representative. To reach a full conversion, double amount of catalyst (120 mg) was used, and reactions were run with three fresh batches of NADH feed. Results are shown in Fig. 5d. After the first run, a conversion of 100% was reached in 1.5 h and the doubled initial reaction rate (0.019 $mM \cdot h^{-1}$) compared to 0.009 $mM \cdot h^{-1}$ (Fig. 5a) confirmed that the reactions were still operating under kinetic control region (i.e., catalyst was not in excess). The unchanged activity in the three successive reactions proved that there was no catalyst deactivation (e.g., leaching, fouling or poisoning). In addition, ICP analysis of the spent catalyst shows that the Pt loading was unchanged (1.10 vs. 1.08 wt. %) before and after reactions (Table 1).

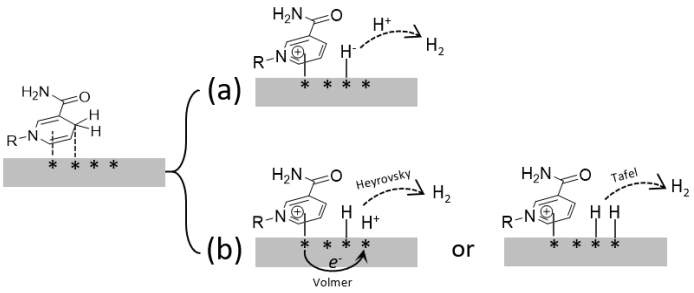

Fig. 4. Plausible reaction pathway of NAD^+ regeneration over a metal surface. The grey rectangle and star (*) represent metal particle and its surface site, respectively.

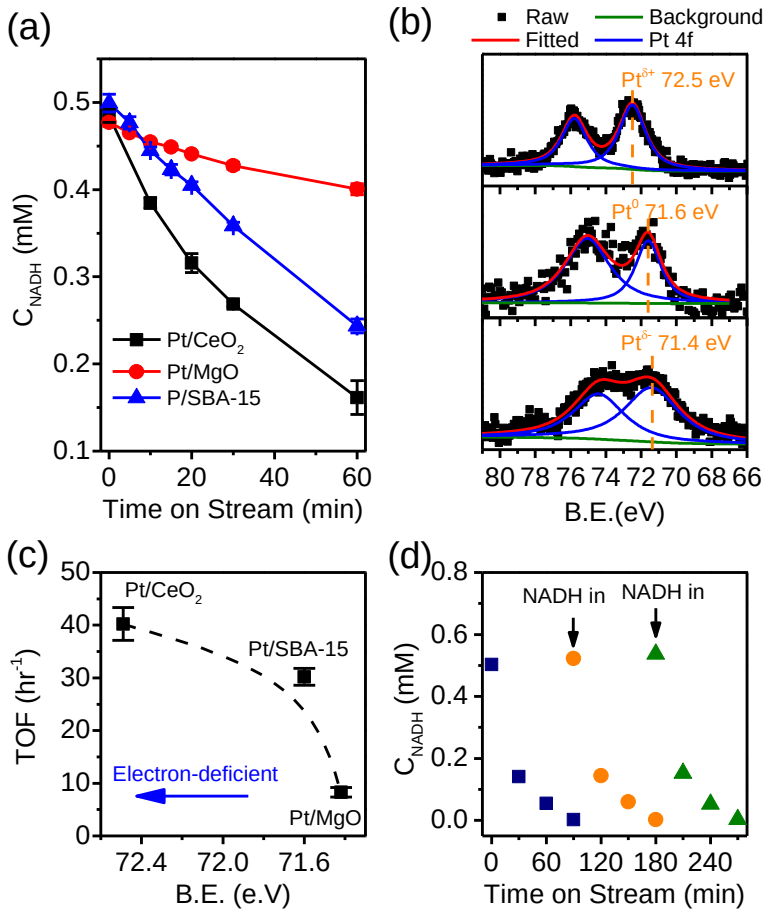

Fig. 5. NADH conversion over Pt/CeO_2, Pt/MgO and Pt/SBA-15 catalysts (a), Pt 4f XPS spectra of the catalysts (b), correlation of TOF with binding energy (c) and catalyst recycle test with Pt/CeO_2 (d). Reaction conditions: 0.5 mM NADH, 100 ml 0.1 M pH 7 PBS, 37 °C, 700 rpm stir, 100 ml·min^{-1} N_2, 60 (for a) or 120 mg (for d) catalyst. Error bars obtained from three independent experiments.

For the first time, we proved the feasibility of H_2 production via H^+-driven NAD^+ regeneration catalyzed by oxide-supported metal catalysts. Pt was shown as the most promising active phase among tested metals (Au, Pd, Ni, Cu and Co, all supported on SBA-15), where NADH was converted to NAD^+ with full selectivity. The trend of metal activity was found following the well-established HER volcano pattern correlated with hydrogen binding energy, confirming a hydrogen-electron transfer mechanism (as opposed to hydride transfer) regarding the hydrogen formation. Electronic structure of the Pt nanoparticles (tuned by using SBA-15, MgO and CeO_2) was important for catalysis where electron-deficient Pt on nonconductive metal oxides favors the activity. This may be due to the lowered hydrogen binding strength with Pt. The results shed light on the design of heterogeneous catalytic systems for proton-driven NAD^+ regeneration as well as a potential route for H_2 production by bio-oxidation.

Acknowledgments

This work was supported by the EPSRC New Horizons grants (EP/V048635/1 and EP/X018172/1).

References

[1] X. Tan, A.J. Chen, B. Wu, et al., Chinese Chem. Lett., 29 (2018) 417-422.
[2] X. Duan, J. Gao, Y.J. Zhou, Chinese Chem. Lett., 29 (2018) 681-686.
[3] H.S. Zurier, J.M. Goddard, Curr. Opin. Food Sci., 37 (2021) 37-44.
[4] S.K. Wu, R. Snajdrova, J.C. Moore, et al., Angew. Chem. Int. Ed., 60 (2021) 88-119.
[5] Z.L. Wang, B.S. Sekar, Z. Li, Bioresour. Technol., 323 (2021) 124551.
[6] Y.S. Lee, K. Lim, S.D. Minteer, Cascaded Biocatalysis and Bioelectrocatalysis: Overview and Recent Advances, in: M.A. Johnson, T.J. Martinez (Eds.), Annual Review of Physical Chemistry, Vol 722021, pp. 467-488.
[7] B. Wiltschi, T. Cernava, A. Dennig, et al., Biotechnol. Adv., 40 (2020) 107520.
[8] J. Li, Y. Tian, Y. Zhou, et al., Trans. Tianjin Univ., 26 (2020) 237-247.
[9] K. Faber, Biocatalytic Applications, in: K. Faber (Ed.) Biotransformations in Organic Chemistry: A Textbook, Springer International Publishing, Cham, 2018, pp. 31-313.
[10] L.S. Vidal, C.L. Kelly, P.M. Mordaka, et al., Biochim. Et Biophys. Acta-Proteins and Proteom., 1866 (2018) 327-347.
[11] Y.G. Zheng, H.H. Yin, D.F. Yu, et al., Appl. Microbiol. Biotechnol., 101 (2017) 987-1001.
[12] G. Rehn, A.T. Pedersen, J.M. Woodley, J. Mol. Catal. B: Enzym., 134 (2016) 331-339.
[13] M.-Q. Xu, F.-L. Li, W.-Q. Yu, et al., Int. J. Biol. Macromol., 144 (2020) 1013-1021.
[14] H. Gao, J. Li, D. Sivakumar, et al., Int. J. Biol. Macromol., 123 (2019) 629-636.

[15] F.-L. Li, Y. Shi, J.-X. Zhang, et al., Int. J. Biol. Macromol., 113 (2018) 1073-1079.
[16] C. Nowak, B. Beer, A. Pick, et al., Front. Microbiol., 6 (2015) 957.
[17] T. Himiyama, M. Waki, Y. Maegawa, et al., Angew. Chem. Int. Ed., 58 (2019) 9150-9154.
[18] C.J. Zhu, Q. Li, L.L. Pu, et al., ACS Catal., 6 (2016) 4989-4994.
[19] R.A. Rodríguez-Hinestroza, C. López, J. López-Santín, et al., Chem. Eng. Sci., 158 (2017) 196-207.
[20] S. Kochius, J.B. Park, C. Ley, et al., J. Mol. Catal. B: Enzym., 103 (2014) 94-99.
[21] S. Kochius, A.O. Magnusson, F. Hollmann, et al., Appl. Microbiol. Biotechnol., 93 (2012) 2251-2264.
[22] B.C. Ma, L. Caire da Silva, S.-M. Jo, et al., ChemBioChem, 20 (2019) 2593-2596.
[23] M. Rauch, S. Schmidt, I.W. Arends, et al., Green Chem., 19 (2017) 376-379.
[24] S. Kochius, Y. Ni, S. Kara, et al., Chempluschem, 79 (2014) 1554-1557.
[25] S. Gargiulo, I.W.C.E. Arends, F. Hollmann, ChemCatChem, 3 (2011) 338-342.
[26] V. Uppada, S. Bhaduri, S.B. Noronha, Curr. Sci., (2014) 946-957.
[27] H. Wu, C. Tian, X. Song, et al., Green Chem., 15 (2013) 1773-1789.
[28] W. Liu, P. Wang, Biotechnol. Adv., 25 (2007) 369-384.
[29] S. Wang, R. Cazelles, W.-C. Liao, et al., Nano Lett., 17 (2017) 2043-2048.
[30] J.-i. Nishigaki, T. Ishida, T. Honma, et al., ACS Sustain. Chem. & Eng., 8 (2020) 10413-10422.
[31] H. Song, C. Ma, L. Wang, et al., Nanoscale, 12 (2020) 19284-19292.
[32] J.W.H. Burnett, H. Chen, J. Li, et al., ACS Appl. Mater. & Interfaces., 14 (2022) 20943-20952.
[33] K. Ganesh, J.B. Joshi, S.B. Sawant, Biochem. Eng. J., 4 (2000) 137-141.
[34] M. Mohanty, R.S. Ghadge, N.S. Patil, et al., Chem. Eng. Sci., 56 (2001) 3401-3408.
[35] R.S. Ghadge, S.B. Sawant, J.B. Joshi, Chem. Eng. Sci., 58 (2003) 5125-5134.
[36] S. Bhagia, C.E. Wyman, R. Kumar, Biotech. for Biofuels, 12 (2019) 1-15.
[37] M.D. Gomes, B.R. Bommarius, S.R. Anderson, et al., Adv. Synth. Catal., 361 (2019) 2574-2581.
[38] M.D. Gomes, R.P. Moiseyenko, A. Baum, et al., Biotechnol. Prog., 35 (2019), e2878.
[39] J.S. Rowbotham, H.A. Reeve, K.A. Vincent, ACS Catal., 11 (2021) 2596-2604.
[40] X. Zhao, S.E. Cleary, C. Zor, et al., Chem. Sci., 12 (2021) 8105-8114.
[41] T. Saba, J.W.H. Burnett, J. Li, et al., Chem. Commun., 56 (2020) 1231-1234.
[42] S. Johnson, P.T. Biochem., 16 (1977) 1175-1183.
[43] H.K. Chenault, G.M. Whitesides, Appl. Biochem. Biotechnol., 14 (1987) 147-197.
[44] P.M. Wood, Biochem. J., 253 (1988) 287-289.
[45] J.K. Nørskov, T. Bligaard, A. Logadottir, et al., J. Electrochem. Soc., 152 (2005) J23-26.
[46] W. Sheng, M. Myint, J.G. Chen, et al., Energy Environ. Sci., 6 (2013) 1509-1512.
[47] Q. Lu, G.S. Hutchings, W. Yu, et al., Nat. Commun., 6 (2015) 6567.
[48] W. Sheng, Z. Zhuang, M. Gao, et al., Nat. Commun., 6 (2015) 5848.
[49] J. Huang, G. Attard, J. Electroanal. Chem., 896 (2021) 115150.
[50] B.C. Song, D. Choi, Y. Xin, et al., Angew. Chem. Int. Ed., 60 (2021) 4038-4042.
[51] Y. Yazawa, N. Takagi, H. Yoshida, et al., Appl. Catal. A: Gen., 233 (2002) 103-112.
[52] Z. Sun, Y. Jiang, W. Wang, et al., ChemCatChem, 12 (2020) 2189-2193.
[53] B.K. Martini, G. Maia, Electrochim. Acta, 391 (2021) 138907.
[54] Y. Cao, D. Wang, Y. Lin, et al., ACS Appl. Energy Mater., 1 (2018) 6082-6088.

Supplementary Material

Supplementary material that may be helpful in the review process should be prepared and provided as a separate electronic file. That file can then be transformed into PDF format and submitted along with the manuscript and graphic files to the appropriate editorial office.